Legendre-spectral Dyson equation solver with super-exponential convergence

(article starts on next page)

Legendre-spectral Dyson equation solver with super-exponential convergence 🄵⊘

Xinyang Dong (ID) ; Dominika Zgid (ID) ; Emanuel Gull (ID) ; Hugo U. R. Strand ✉ (ID)

Check for updates

⤓ CHORUS

View Online   Export Citation

Legendre-spectral Dyson equation solver with super-exponential convergence Ⓕ

Xinyang Dong,[1] ⓘD Dominika Zgid,[1,2] ⓘD Emanuel Gull,[1] ⓘD and Hugo U. R. Strand[3,4,a)] ⓘD

AFFILIATIONS

[1] Department of Physics, University of Michigan, Ann Arbor, Michigan 48109, USA
[2] Department of Chemistry, University of Michigan, Ann Arbor, Michigan 48109, USA
[3] Department of Physics, Chalmers University of Technology, SE-412 96 Gothenburg, Sweden
[4] Center for Computational Quantum Physics, The Flatiron Institute, New York, New York 10010, USA

[a)]Author to whom correspondence should be addressed: hugo.strand@gmail.com

ABSTRACT

Quantum many-body systems in thermal equilibrium can be described by the imaginary time Green's function formalism. However, the treatment of large molecular or solid *ab initio* problems with a fully realistic Hamiltonian in large basis sets is hampered by the storage of the Green's function and the precision of the solution of the Dyson equation. We present a Legendre-spectral algorithm for solving the Dyson equation that addresses both of these issues. By formulating the algorithm in Legendre coefficient space, our method inherits the known faster-than-exponential convergence of the Green's function's Legendre series expansion. In this basis, the fast recursive method for Legendre polynomial convolution enables us to develop a Dyson equation solver with quadratic scaling. We present benchmarks of the algorithm by computing the dissociation energy of the helium dimer He_2 within dressed second-order perturbation theory. For this system, the application of the Legendre spectral algorithm allows us to achieve an energy accuracy of $10^{-9} E_h$ with only a few hundred expansion coefficients.

Published under license by AIP Publishing. https://doi.org/10.1063/5.0003145

I. INTRODUCTION

The equilibrium properties of many-body quantum systems can be described by the finite temperature imaginary-time Green's function formalism,[1] which is widely applicable to condensed matter physics, quantum chemistry, and materials science. Applications include numerical methods for low energy effective model Hamiltonians such as lattice Monte Carlo,[2] dynamical mean field theory[3] and its extensions,[4–6] and diagrammatic Monte Carlo.[7] *Ab initio* calculations using the random phase approximation,[8] self-consistent second order perturbation theory,[9–17] Hedin's *GW* approach,[18–26] and self-energy embedding theory[27–33] can also be formulated in imaginary time.

While the finite temperature Green's function formalism is very successful in applications to model Hamiltonians, its applicability to quantum chemistry and materials science remains limited to simple molecular and periodic problems. This is due to the necessity of simultaneously describing both the core and valence orbitals, which results in an energy scale that is difficult to describe

by a single imaginary time/frequency grid. A simple equidistant Matsubara grid would contain millions of points, thus making the storage and manipulation of the Green's functions computationally costly. In contrast, a grid with only a small number of equidistant points will result in a poorly converged energy or density matrix, making calculations with μHartree precision challenging. Such precision is necessary in applications where the evaluation of interaction energies,[34–37] energies of conformers,[38] or energies of high-lying excited states[39,40] is needed. Consequently, it is important to develop a compact representation that yields highly converged properties.

With the standard approach using equidistant Matsubara frequency[41] grids with finite frequency cutoff, the imaginary time Green's function only converges to the analytical result linearly in the number of Matsubara frequencies. Amending the representation with a low order high frequency expansion results in polynomial convergence.[42–44] In practice, this is problematic, since for systems with a wide range of energy scales, the number of coefficients is controlled by the largest energy scale.[14] Alternatives such

TABLE I. Overview of Green's function representation approaches in both Matsubara frequency space and imaginary time combined with the scaling of solvers for the Dyson equation. Where no convergence is listed, the scaling either involves additional parameters or is unknown.

Domain	Basis	Convergence	Compactness	Dyson scaling
Matsubara frequency	Finite frequency cutoff	$\mathcal{O}(1)$	Poor	$\mathcal{O}(N)$
	Tail correction, pth order[42–44]	$\mathcal{O}(N^{-p})$	Fair	...
	Spline grid[14]	...	Good	...
Both frequency and time	Sparse sampling[52]	...	See Ref. 52[a]	$\mathcal{O}(N)$
	Minimax isometry[53]	...	See Ref. 53	$\mathcal{O}(N)$
Imaginary time	Uniform mesh	$\mathcal{O}(N^{-1})$	Poor	$\mathcal{O}(N^3)$
	Power mesh[45,46,58]	...	Fair	$\mathcal{O}(N^3)$
Orthogonal functions	Intermediate representation[49–51]	$\lesssim \mathcal{O}(e^{-N})$	Excellent	No
	Chebyshev polynomials[48]	$\lesssim \mathcal{O}(e^{-N})$	Very good	$\mathcal{O}(N^3)$
	Legendre polynomials (this work)	$\lesssim \mathcal{O}(e^{-N})$[47]	Very good	$\mathcal{O}(N^2)$

[a]The compactness of the sparse sampling approach depends on the real-time basis employed.

as uniform power meshes have had some success.[45,46] However, the most compact representations are achieved using a set of (orthogonal) continuous basis functions directly in imaginary time, such as orthogonal polynomials[47,48] or numerical basis functions.[49–53] The convergence of such a representation is faster than exponential,[47,48] and asymptotically superior to any polynomially converging representation.

In all imaginary time methods, a central step besides the solution of the impurity problem is the solution of the Dyson equation for the single particle Green's function.[54–57] In the Matsubara frequency representation,[41] the Dyson equation is diagonal and can be readily solved. However, the solution is plagued by the polynomial convergence with respect to the number of frequency coefficients used. In imaginary time, the Dyson equation is a non-trivial integro-differential equation with a mixed boundary condition. Recently, an algorithm for solving the Dyson equation in imaginary time using the Chebyshev polynomials has been presented.[48] This algorithm preserves the exponential convergence of the orthogonal polynomial expansion.[47] However, the central convolution step has a cubic scaling in the expansion order N_L, $\sim \mathcal{O}(N_L^3)$, which limits the applicability of the algorithm.

The development of compact representations and algorithms for solving the Dyson equation is an active field of research (see Table I for an overview of the state-of-the-art methods). For a recent development, see Ref. 53.

In this paper, we present a Legendre spectral method for solving the Dyson equation with super-exponential convergence and a convolution that scales quadratically $\sim \mathcal{O}(N_L^2)$, one order better than previous formulations.[48] The super-exponential convergence allows us to achieve an energy accuracy of $10^{-9} E_h$ in a realistic quantum chemistry system with a few hundred expansion coefficients. We show this in a proof-of concept benchmark: computing the dissociation energy of He_2 using self-consistent second-order perturbation theory, taking both the zero temperature and the complete basis limit.

This paper is organized as follows: In Sec. II, we introduce the Dyson equation. In Sec. III, we present our Legendre spectral method. In Secs. IV and V, we apply our method to a realistic quantum chemistry problem, the dissociation energy of the noble gas He_2. In Sec. VI, we present conclusions.

II. THEORY

The imaginary time single particle Green's function G is defined on the interval $\tau \in [-\beta, \beta]$, $G \equiv G(\tau)$, where β is the inverse temperature $\beta = 1/T$. It obeys the periodicity condition $G(-\tau) = \xi G(\beta - \tau)$, with $\xi = +1$ (-1) for bosons (fermions), making it an (anti-)periodic function with a step discontinuity at $\tau = 0$ [see Fig. 1(a)]. The imaginary time Dyson equation for $G(\tau)$ is[54–57]

$$[-\partial_\tau - h]G(\tau) - \Sigma * G = 0, \qquad (1)$$

where h is the single particle energy and Σ is the self-energy, which accounts for all many-body interactions. We note in passing that $\Sigma(\tau)$ has the same periodicity as $G(\tau)$. The boundary condition for Eq. (1) is $G(0) - \xi G(\beta) = -1$, and the Fredholm type[59] imaginary time convolution is defined as $\Sigma * G \equiv \int_0^\beta d\bar{\tau}\, \Sigma(\tau - \bar{\tau}) G(\bar{\tau})$.

Analytically, the Dyson equation [Eq. (1)] can be solved using the Fourier series expansion,

$$G(\tau) = \frac{1}{\beta} \sum_{n=-\infty}^{\infty} e^{-i\omega_n \tau} G(i\omega_n), \quad G(i\omega_n) = \int_0^\beta d\tau\, e^{i\omega_n \tau} G(\tau),$$

where the Matsubara frequencies $i\omega_n$ are given by $i\omega_n \equiv i\frac{\pi}{\beta}(2n + \eta)$ with $\eta = (1 - \xi)/2$ and n integers.[54–57] In Matsubara frequency space, the Dyson equation [Eq. (1)] is diagonal,[41]

$$[i\omega_n - h - \Sigma(i\omega_n)]G(i\omega_n) = 1. \qquad (2)$$

Numerically, however, the discontinuity at $\tau = 0$ results in a slow asymptotic decay $G(i\omega_n) \sim (i\omega_n)^{-1}$ as $i\omega_n \to \pm i\infty$ [see Fig. 1(b)].
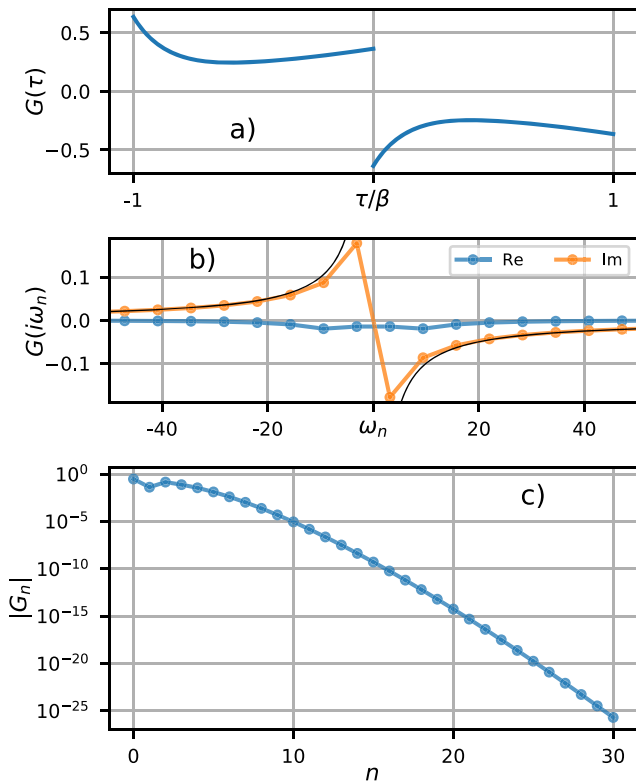
FIG. 1. Single particle Green's function in (a) imaginary time $G(\tau)$, (b) Matsubara frequency $G(i\omega_n)$ [with $(i\omega_n)^{-1}$ black line], and (c) Legendre expansion coefficients G_n for site one in the fermionic two level system with the second quatization Hamiltonian $H = -\mu c_1^\dagger c_1 + V(c_1^\dagger c_2 + c_2^\dagger c_1) + \epsilon c_2^\dagger c_2$ at inverse temperature $\beta = 1$, where $c_i^\dagger$ creates and c_i annihilates a fermion at site i and $\mu = -3$, $\epsilon = 3.3$, and $V = 4$.

FIG. 2. Error in density Δn as a function of Legendre expansion order N_L and number of Matsubara frequencies N_ω for the same system as in Fig. 1.

This prevents a naïve finite frequency $|n| < N_\omega$ approximation $G(\tau) \approx \frac{1}{\beta} \sum_{|n|<N_\omega} e^{-i\omega_n\tau} G(i\omega_n)$ from converging in N_ω [the maximal error in $G(\tau)$ scales as $\sim \mathcal{O}(N_\omega^0) = \mathcal{O}(1)$]. The standard solution to this problem is to use a finite number p of high-frequency "tail" coefficients $\bar{G}_k$ to approximate $G(i\omega_n) \approx \sum_{k=1}^{p} \bar{G}_k/(i\omega_n)^k$ for $|n| > N_\omega$, where the known asymptotic decay implies $\bar{G}_1 = 1$. This type of tail correction procedure gives polynomial convergence in $G(\tau)$ with the power determined by the order p of the tail expansion $\sim \mathcal{O}(N_\omega^{-p})$ [see, e.g., Refs. 42–44]. In Fig. 2, this is shown for the case of $p = 3$ using the TRIQS library.[60]

Since $G(\tau)$ is continuous on $\tau \in [0, \beta]$, it can be much more efficiently represented by a finite orthogonal polynomial expansion,

$$G(\tau) \approx \sum_{n=0}^{N_L} G_n L_n[x(\tau)], \qquad (3)$$

where $L_n[x]$ are Legendre polynomials defined on $x \in [-1, 1]$ and $x(\tau) = \frac{2\tau}{\beta} - 1$. The Legendre coefficients G_n have a faster than exponential asymptotic decay[47] [see Fig. 1(c)]. This also causes the
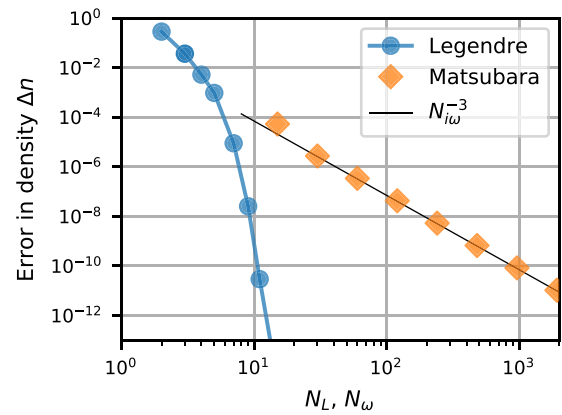
finite N_L expansion at the right-hand side of Eq. (3) to converge faster than exponential $\lesssim \mathcal{O}(e^{-N_L})$ to the analytical $G(\tau)$.

III. LEGENDRE SPECTRAL METHOD

Here, we develop a Legendre spectral method for solving the Dyson equation [Eq. (1)], reformulating the integro-differential equation in the space of Legendre coefficients G_n [Eq. (3)]. In the space of a finite Legendre expansion of order N_L, Eq. (1) is cast to a linear equation system,

$$\sum_{n=0}^{N_L} \left(-D_{kn} - h\mathbf{1}_{kn} - [\Sigma *]_{kn} \right) G_n = \mathbf{0}_k, \qquad (4)$$

where terms with one and two indices are vectors and matrices in Legendre coefficient space. The last row of the left-hand side of the matrix is modified to enforce the boundary condition of Eq. (1). The resulting method has faster than exponential convergence and quadratic scaling $\sim \mathcal{O}(N_L^2)$, one order better than previous approaches.[48]

The differential operator ∂_τ in Eq. (1) acting on the Legendre polynomials takes the form[61]

$$\partial_\tau L_n[x(\tau)] = \frac{2}{\beta} \partial_x L_n(x) = \frac{2}{\beta} \sum_{k=0,\,k+n\ \text{odd}}^{n-1} (2k+1) L_k(x)$$

$$= \sum_k D_{kn} L_k(x). \qquad (5)$$

Hence, the derivative matrix D_{kn} in Eq. (4) is given by

$$\frac{\beta}{2} D_{kn} \equiv \begin{cases} 2k+1, & 0 \le k \le n, k+n\ \text{odd}, \\ 0, & \text{elsewhere} \end{cases} \qquad (6)$$

and is upper triangular (see Fig. 3). Using $L_n(\pm 1) = (\pm 1)^n$, the Dyson equation boundary condition can be written as

$$-1 = G(0) - \xi G(\beta) = \sum_n \left((-1)^n - \xi \right) G_n. \qquad (7)$$
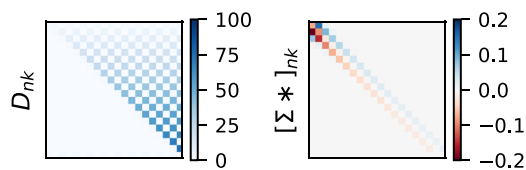
05 July 2024 10:32:15

FIG. 3. Matrix structure of the spectral derivative operator D_{kn} and the convolution operator $[\Sigma*]_{kn}$ for $\epsilon = 1$ and $\Sigma(\tau) = e^{-\epsilon\tau}(\xi e^{-\epsilon\beta} - 1)^{-1}$ at $\beta = 1$ and $\xi = -1$ (fermions).

A. Spectral convolution

The imaginary time convolution $[\Sigma * G]$ in the Dyson equation [Eq. (1)] can be separated into the two terms of Volterra type,

$$[\Sigma * G](\tau) = \int_0^\beta d\tau' \Sigma(\tau - \tau') G(\tau')$$
$$= \int_0^\tau d\tau' \Sigma(\tau - \tau') G(\tau') + \int_\tau^\beta d\tau' \xi \Sigma(\beta + \tau - \tau') G(\tau'),$$

(8)

using the periodicity property $\Sigma(-\tau) = \xi\Sigma(\beta - \tau)$. In Eq. (8), $\Sigma(\tau)$ is only evaluated for $\tau \in [0, \beta]$, avoiding the discontinuity at $\tau = 0$.

In Legendre coefficient space, the convolution operator $[\Sigma *]$ can be written as a sum of two matrices $B_{kn}^{\lessgtr}$, representing the two Volterra terms [Eq. (8)],

$$[\Sigma *]_{kn} \equiv B_{kn}^< + \xi B_{kn}^>.$$

(9)

Stable recursion relations for $B_{nk}^{\lessgtr}$ have been derived by Hale and Townsend[62] using the Fourier connection between Legendre polynomials and spherical Bessel functions. Since the derivation is detailed in Ref. 62, we only state the result specialized to the imaginary time convolution in Eq. (8) here and provide a derivation in the Appendix.

The coefficients are related by the recursion relation,

$$B_{k,n+1}^{\lessgtr} = -\frac{2n+1}{2k+3} B_{k+1,n}^{\lessgtr} + \frac{2n+1}{2k-1} B_{k-1,n}^{\lessgtr} + B_{k,n-1}^{\lessgtr},$$

(10)

which for each column require two previous columns to be known. The recursion is only stable for the lower triangular coefficients in $B_{kn}^{\lessgtr}$. The upper triangular coefficients are computed using the transpose relation,

$$B_{k,n}^{\lessgtr} = (-1)^{n+k} \frac{2k+1}{2n+1} B_{n,k}^{\lessgtr}.$$

(11)

The two first columns are given by the starting relations,

$$B_{k,0}^{\lessgtr} = \begin{cases} \Sigma_0 \pm \frac{\Sigma_1}{3}, & k = 0, \\ \pm\left(\frac{\Sigma_{k-1}}{2k-1} - \frac{\Sigma_{k+1}}{2k+3}\right), & k \geq 1, \end{cases}$$

$$B_{k,1}^{\lessgtr} = \mp B_{k,0}^{\lessgtr} + \frac{B_{k-1,0}^{\lessgtr}}{2k-1} - \frac{B_{k+1,0}^{\lessgtr}}{2k+3}, \quad k \geq 1,$$

(12)

with the special case for $k = 0$, $B_{0,1}^{\lessgtr} = \mp B_{1,0}^{\lessgtr}/3$, using the Legendre coefficients Σ_n of the self-energy Σ [cf. Eq. (3)].

B. Convergence and scaling

Since each coefficient in $B_{kn}^{\lessgtr}$ can be computed in $\mathcal{O}(1)$ operations, the scaling of the convolution matrix construction is $\sim \mathcal{O}(N_L^2)$. The self-energy $\Sigma(\tau)$ is a smooth function with asymptotic exponentially decaying Legendre coefficients, which causes the entries of the dominantly diagonal spectral convolution operator $[\Sigma *]_{kn}$ to decay exponentially both along and away from the diagonal (see Fig. 3).

The numerical solution of $G(\tau)$ from the Dyson equation constructed in terms of the linear system in Eq. (4) converges faster than exponentially to the analytical solution, with the increased number of Legendre coefficients N_L (see Fig. 2). This is in stark contrast to the polynomial convergence of the standard Matsubara tail approach[42–44] (also shown in Fig. 2).

C. Imaginary time transform

To retain the high accuracy of the Legendre spectral Dyson solver, the method has to be complemented with stable transforms between Legendre coefficients and imaginary time,

$$G_n = \sum_{i=0}^{N_L} S_{ni} G(\tau_i), \quad G(\tau_i) = \sum_{n=0}^{N_L} L_{in} G_n.$$

(13)

To construct the well-conditioned transform matrices S_{ni} and L_{in}, we employ the Legendre quadrature and the Legendre–Gauss–Lobatto points $x_i \in \{x : (1 - x^2)L_{N_L}'(x) = 0\}$, $x_0 = -1$, $x_N = 1$, re-scaled to the imaginary time interval $[0, \beta]$, $\tau_i = \beta\frac{x_i+1}{2}$. Using x_i, the matrices S_{ni} and L_{in} can be directly constructed (avoiding matrix inversion),

$$L_{in} = L_n(x(\tau_i)), \quad S_{ni} = \frac{\beta}{2W_n}\omega_i L_n(x(\tau_i)),$$

(14)

where $\int_{-1}^1 dx L_n(x)L_m(x) = \delta_{nm}\frac{2}{2n+1} \equiv \delta_{nm}W_n$ and $\omega_i = \frac{2}{N(N+1)}\frac{1}{L_{N_L}(x_i)^2}$ (see, e.g., Refs. 61 and 63).

IV. APPLICATION (GF2)

As a proof of concept application of the Legendre spectral Dyson solver developed in this paper, we employ the solver in a quantum chemistry setting using a Gaussian basis set. We will employ self-consistent second order perturbation theory, also known as GF2,[9–17] which has seen a revival in recent years, both in *ab initio* condensed matter applications[8,15] and in quantum chemistry[11,16,58,64] in combination with embedding methods.[29] Our implementation is built on the Coulomb integrals of the pyscf library.[65]

In the resulting non-orthogonal basis set, the Dyson equation takes the form

$$\sum_j [S_{ij}(\partial_\tau - \mu) + F_{ij} + \Sigma_{ij}*] G_{jk}(\tau) = \mathbf{0},$$

(15)

where i, j, k are orbital indices, S_{ij} is the overlap matrix, and F_{ij} is the so-called Fock matrix, $F_{ij} \equiv h_{ij} + \Sigma_{ij}^{(HF)}$. The boundary condition for this equation is $\sum_j (G_{ij}(0) - \xi G_{ij}(\beta)) \cdot S_{jk} = -\mathbf{1}_{ik}$. Here, the single particle term h_{ij} accounts for electronic kinetic and nuclear-electronic matrix elements, and the Hartree–Fock self-energy $\Sigma_{ij}^{(HF)}$ is given by

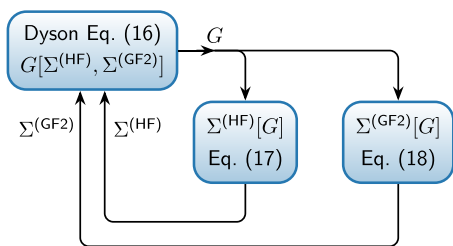$$\Sigma_{ij}^{(HF)} = \sum_{kl} P_{kl}(v_{ijkl} - v_{ilkj}/2),$$

(16)

FIG. 4. Schematic of the GF2-self-consistency loop.

where P_{ij} is the density matrix $P_{ij} = -2G_{ij}(\beta)$ and v_{ijkl} is the electron–electron Coulomb repulsion integral.

In GF2, the imaginary-time-dependent part of the self-energy $\Sigma(\tau)$ is approximated with the second order self-energy diagram using the full electron Greens function G, $\Sigma \approx \Sigma^{(GF2)}[G]$, where

$$\Sigma_{ij}^{(GF2)}(\tau) = \sum_{klmnpq} G_{kl}(\tau)G_{mn}(\tau)G_{pq}(\beta-\tau)$$
$$\times v_{impk}(2v_{jnlq} - v_{jlnq}). \quad (17)$$

The evaluation of $\Sigma^{(GF2)}(\tau)$ for fixed τ scales as $\sim \mathcal{O}(N^5)$,[64] where N is the number of atomic orbitals.

Solving for the GF2 Green's function, G amounts to solving Eqs. (15)–(17), which is a highly non-linear problem. To find the solution, we perform self-consistent iterations (see Fig. 4 for a schematic picture). The inner loop solves the Dyson equation [Eq. (15)] and updates the Hartree–Fock self-energy $\Sigma^{(HF)}$ [Eq. (16)] until convergence (in the Fock-matrix F). At convergence in F, one step of the outer loop is performed by re-evaluating the GF2 self-energy $\Sigma^{(GF2)}$ [Eq. (17)] and computing the relative change in total energy E. If the change is above a fixed threshold, the inner loop is started again. To compute the inter molecular energies, which is an energy difference, we need a threshold of 10^{-10}.

The total energy E of the system is given by

$$E = \frac{1}{2}\text{Tr}[(h+F)P] + \text{Tr}[\Sigma * G] + E_{nn}, \quad (18)$$

where E_{nn} is the nuclei–nuclei Coulomb energy. The imaginary time trace $\text{Tr}[\cdot]$ is defined as $\text{Tr}[A] \equiv -\sum_i A_{ii}(\beta)$,[44,66] and the $\Sigma * G$ convolution is computed with the spectral Legendre convolution as in Eq. (4).

V. RESULTS

The faster than exponential convergence of the Legendre spectral Dyson solver [Eq. (4)] is particularly suited for high precision calculations. A prime example is the computation of the binding energy D_e in noble-gas dimers, where the weak bonding requires high precision calculations of total energies. The binding energy D_e is obtained from the minimum of the interaction energy $E_{int}(r)$ as a function of atomic separation r,

$$D_e \equiv -E_{int}(r_e) \equiv -\min_r E_{int}(r), \quad (19)$$

where r_e is the equilibrium atomic distance. The interaction energy E_{int} is, in turn, given by

$$E_{int}(r) \equiv E_{A_2}(r) - 2E_A(r), \quad (20)$$

where E_{A_2} is the total energy of the dimer and E_A is the total energy of the single atom (the monomer) evaluated using the standard counterpoise correction.[67] In the noble gases, the total energies E_A and E_{A_2} are of the order of Hartrees ($\sim E_h \equiv 1$ Hartree), while the binding energy D_e is of the order of tens of micro-Hartrees ($\sim 10\mu E_h$), hence requiring high precision calculation of the total energies.

We use He$_2$ as a prototype system since there exist published reference results for the binding energy D_e and equilibrium distance r_e calculated with Hartree–Fock (HF), second-order Moller–Plesset perturbation theory (MP2), coupled cluster singles doubles (CCSD) theory, and coupled cluster singles doubles and non-iterative perturbative triples [CCSD(T)] theory.[68] The MP2 method is closely related to GF2 and uses the second order self-energy [Eq. (17)] evaluated at the HF Green's function $G^{(HF)}$, $\Sigma^{(MP2)} \equiv \Sigma^{(GF2)}[G^{(HF)}]$. However, note that the prefactors in the total energy differ.[10,69]

Figure 5 shows $E_{int}(r)$ (and $-D_e$) of He$_2$ computed with HF, MP2, and GF2 in the aug-cc-pvqz basis together with CCSD and CCSD(T) reference results on D_e.[68] The GF2 results are obtained by fitting a 4th order polynomial to 21 r-points of $E_{int}(r)$ computed in a 0.1 Bohr range centered around the minimum at r_e. The GF2 results are obtained using the Legendre spectral Dyson solver, while HF and MP2 are computed using pyscf.[65] As shown in Fig. 5, He$_2$ does not bind within the Hartree–Fock approximation, which gives a strictly positive interaction energy. Compared to MP2 our GF2 results are a considerable improvement using the coupled cluster CCSD and CCSD(T) as a reference.
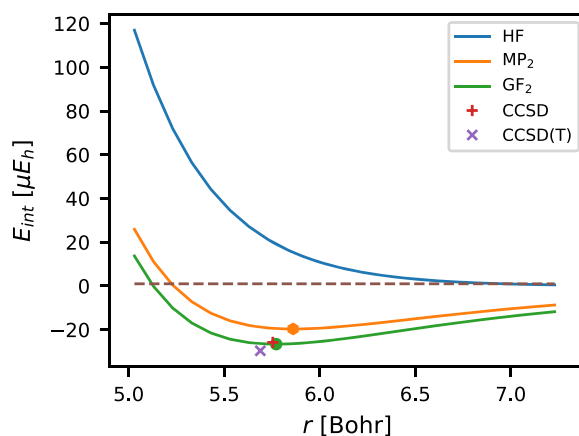

FIG. 5. Interaction energy E_{int} as a function of atomic distance r of He$_2$ with basis aug-ccpvqz using HF, MP2, and GF2. The HF and MP2 results are computed with pyscf;[65] the GF2 results are computed using $\beta = 50\,E_h^{-1}$, $N_\tau = 192$. The CCSD and CCSD(T) results are from Ref. 68.

A. Complete basis set limit

In order to extrapolate the results to the complete basis set (CBS) limit,[70,71] we repeat the calculations using the augmented correlation consistent (aug-cc-pv$n$z) basis set series, with n = d, t, q, 5 (i.e., n = 2, 3, 4, 5).[72–74] This series has been shown to enable accurate extrapolation of a number of properties due to its systematic convergence in n.[70,75–85]

In Table II, we summarize the binding energy D_e and equilibrium distance r_e of He$_2$ computed by MP2, CCSD, CCSD(T), and GF2 using the aug-cc-pv{d,t,q,5}z basis sets. The aug-cc-pv{d,t,q,5}z GF2 energies are computed at $\beta = 50\,E_h^{-1}$ using N_τ = 128, 160, 192, and 250 τ-points, respectively. The convergence in N_τ is imposed so that the absolute values of the elements in highest Legendre coefficient matrix are smaller than 10^{-10}. The zero temperature convergence (at $\beta = 50\,E_h^{-1}$) is ensured by requiring that the finite temperature MP2 total energy differs by less than 0.1 nHartree compared to the zero temperature MP2 total energy from pyscf.

We note that the number of τ-points N_τ used for the aug-cc-pv{d,t,q,5}z basis sets is of the same order as the number of atomic orbitals N. Hence, the scaling of GF2, $\sim \mathcal{O}(N_\tau \cdot N^5)$, is comparable to the scaling of CCSD, $\sim \mathcal{O}(N^6)$. As given in Table II, the accuracy of the GF2 result for D_e is comparable to that of CCSD when compared to that of CCSD(T), while the CCSD result for r_e is closer to the CCSD(T) result than that of GF2. This makes GF2 a considerable improvement over MP2.

With the systematic convergence of D_e and r_e as a function of basis set size n, it is possible to extrapolate to the complete basis limit $n \to \infty$.[68] We extrapolate D_e and r_e using our GF2 aug-ccpv{t,q,5}z results by fitting the exponential model: $A \cdot e^{-B(n-2)} + C$, proposed in Ref. 68, where A, B, and C are parameters. The applicability of the model is checked by a logarithmic plot (see Fig. 6). The resulting CBS limit of our GF2 results is $D_e \approx 29.67\,\mu E_h$ and $r_e \approx 5.680\,a_0$ (see also Table II).
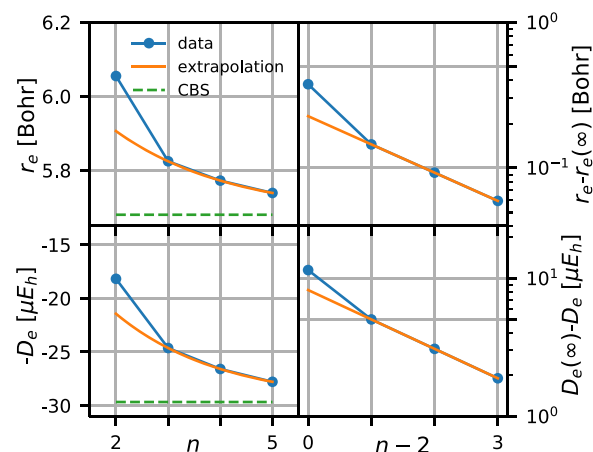

FIG. 6. Basis extrapolation of equilibrium distance (r_e) and dissociation energy (D_e) He$_2$ with basis aug-ccpvnz with n = 2, 3, 4, 5. Left panels: raw data and fitting. Right panels: check of fitting results.

VI. CONCLUSION AND OUTLOOK

We introduce a Legendre-spectral algorithm for solving the Dyson equation in Legendre coefficient space. By staying in Legendre-coefficient space, the algorithm converges super exponentially with respect to the number of Legendre coefficients N_L used to represent the imaginary time Green's function.[47] This is in stark contrast to the Matsubara frequency space based approach with only polynomial convergence.[42–44] The exponential convergence is shared with a recently presented Chebyshev polynomial based algorithm,[48] where the convolution scales as $\sim \mathcal{O}(N_L^3)$. Currently, there is no known algorithm for Chebyshev series that can compute the convolution term with the same efficiency as in the Legendre series.[62] Our work goes beyond this, employing a Legendre convolution with $\mathcal{O}(N_L^2)$ scaling and enabling the application to larger *ab initio* systems.

To benchmark the algorithm, we apply it to the quantum chemistry computation of the dissociation energy of the noble gas He$_2$ using self-consistent second order perturbation theory (GF2). The exponential convergence of our algorithm allows us to reach the required $10^{-9} E_h$ zero temperature total-energy precision using only 100–200 Legendre coefficients in the Dunning basis series aug-ccpv$n$z.[72–74]

The algorithm is also relevant for condensed matter *ab initio* applications in periodic systems that require high precision, such as GF2[9–17] and Hedin's GW.[18–26] This is a promising venue for future research.

TABLE II. Dissociation energies D_e (top) and equilibrium distances r_e computed by MP2, CCSD, CCSD(T), and GF2 with the basis sets aug-cc-pv$n$z, with n = d, t, q, 5. The MP2, CCSD, and CCSD(T) results are from Ref. 68.

$D_e\ (\mu E_h)$	MP2	CCSD	CCSD(T)	GF2
aug-ccpvdz	12.69	16.78	18.57	18.17
aug-ccpvtz	17.97	23.77	27.10	24.63
aug-ccpvqz	19.66	25.79	29.64	26.59
aug-ccpv5z	20.71	27.09	31.25	27.79
CBS	22.98	30.06	34.70	29.67

r_e (Bohr)	MP2	CCSD	CCSD(T)	GF2
aug-ccpvdz	6.1680	6.0580	6.0086	6.0547
aug-ccpvtz	5.9175	5.8060	5.7452	5.8244
aug-ccpvqz	5.8606	5.7546	5.6891	5.7722
aug-ccpv5z	5.8244	5.7210	5.6537	5.7388
CBS	5.769	5.672	5.607	5.680

Werner, and Hiroshi Shinaoka, who took part in early discussion on Green's function representations, which guided the development of the method, and (v) Antoine Georges, Olivier Parcollet, Manuel Zingl, Alexandru Georgescu, Igor Krivenko, and Nils Wentzell, who contributed through discussions and contributions to the TRIQS project. E.G. and X.D. were supported by the Simons Collaboration on the many-electron problem. D.Z. acknowledges support from Grant No. NSFCHE-1453894. The Flatiron Institute is a division of the Simons Foundation.

APPENDIX: CONVOLUTION MATRIX

In this appendix, we derive Eqs. (10)–(12) in the main text. The derivation follows Ref. 62 but with more details for both integrals in Eq. (8).

1. Convolution and Fourier transform

The convolution of two continuous integrable functions is defined as[62]

$$h(x) = (f * g)(x) \equiv \int_{-\infty}^{\infty} dt\, f(t) g(x - t). \tag{A1}$$

With the assumption f and g being periodic functions, their Fourier transform can be written as

$$\mathcal{F}\{f\}(\omega) = \int_{-\infty}^{\infty} dx\, e^{-i\omega x} f(x), \tag{A2}$$

$$\mathcal{F}^{-1}\{f\}(x) = \frac{1}{2\pi} \int_{-\infty}^{\infty} dx\, e^{i\omega x} f(x), \tag{A3}$$

which satisfy the Fourier inversion theorem $\mathcal{F}^{-1}\{\mathcal{F}\{f\}\} = f$ and convolution theorem,[86]

$$\mathcal{F}\{f * g\} = \mathcal{F}\{f\} \cdot \mathcal{F}\{g\}. \tag{A4}$$

2. Legendre polynomials

The Legendre polynomials $P_n(x)$ can be defined recursively using the three term recurrence relation,

$$\begin{aligned} P_0(x) = 1, \quad P_1(x) = x, \\ (n+1)P_{n+1}(x) = (2n+1)x P_n(x) - n P_{n-1}(x). \end{aligned} \tag{A5}$$

They are orthogonal on $[-1, 1]$,

$$\int_{-1}^{1} dx\, P_m(x) P_n(x) = \delta_{m,n} \frac{2}{2n+1}, \tag{A6}$$

and the derivatives satisfy the recurrence relation,

$$(2n+1)P_n(x) = \frac{d}{dx}[P_{n+1}(x) - P_{n-1}(x)]. \tag{A7}$$

The Fourier transform and inverse Fourier transform of the Legendre polynomials can be expressed in terms of Bessel functions of the first kind,

$$\mathcal{F}\{P_n\} = \int_{-1}^{1} dx\, e^{-i\omega x} P_n(x) = 2(-i)^n j_n(\omega), \tag{A8}$$

$$\mathcal{F}^{-1}\{P_n\} = \int_{-1}^{1} dx\, e^{i\omega x} P_n(x) = 2i^n j_n(\omega), \tag{A9}$$

where $j_n(z)$ is the nth spherical Bessel function and $P_n = 0$ outside $[-1, 1]$.

By combining Eqs. (A4) and (A8), the convolution of Legendre polynomials can be expressed in terms of Bessel functions,

$$(P_m * P_n)(x) = \frac{2(-i)^{m+n}}{\pi} \int_{-\infty}^{\infty} d\omega\, e^{i\omega x} j_m(\omega) j_n(\omega). \tag{A10}$$

This is the central observation of Ref. 62 that enables the derivation of recursion relations for the Legendre polynomial convolution.

The main property of spherical Bessel functions used is the three term recurrence relation,

$$\begin{aligned} j_{-1}(z) = \frac{\cos z}{z}, \quad j_0(z) = \frac{\sin z}{z}, \\ j_{n+1}(z) = \frac{2n+1}{z} j_n(z) - j_{n-1}(z), \quad n \geq 0. \end{aligned} \tag{A11}$$

The convolution equation [Eq. (A1)] can be computed by replacing the two continuous function $f(x)$ and $g(x)$ on the bounded interval with polynomial approximates $f_M(x)$ and $g_N(x)$ of sufficiently high degree. With two Legendre series $f_M(x)$ and $g_N(x)$ supported on $x \in [-1, 1]$,

$$f_M(x) = \sum_{m=0}^{M} \alpha_m P_m(x), \quad g_N(x) = \sum_{n=0}^{N} \beta_n P_n(x). \tag{A12}$$

Equation (A1) becomes

$$\begin{aligned} h(x) = (f_M * g_N)(x) = \int_{\max(-1,x-1)}^{\min(1,x+1)} dt\, f_M(t) g_N(x-t) \\ = \int_{-1}^{x+1} dt\, f_M(t) g_N(x-t) + \int_{x-1}^{1} dt\, f_M(t) g_N(x-t), \end{aligned} \tag{A13}$$

which can be computed separately in two integration domains $x \in [-2, 0]$ and $x \in [0, 2]$ (see Fig. 4.1 in Ref. 62).

a. First interval $x \in [-2, 0]$

For $x \in [-2, 0]$, we have $h(x) = h^<(x)$, where

$$h^<(x) = \int_{-1}^{x+1} dt\, f_M(t) g_N(x-t) = \sum_{k=0}^{M+N+1} \gamma_k^< P_k(x+1). \tag{A14}$$

Using the orthogonality of Legendre polynomials [Eq. (A6)], we have

$$\begin{aligned} \gamma_k^< = \frac{2k+1}{2} \int_{-2}^{0} dx\, P_k(x+1) \int_{-1}^{x+1} dt\, f_M(t) g_N(x-t) \\ = \sum_{n=0}^{N} \beta_n \frac{2k+1}{2} \sum_{m=0}^{M} \alpha_m \int_{-2}^{0} dx\, P_k(x+1) \\ \times \int_{-1}^{x+1} dt\, P_m(t) P_n(x-t), \end{aligned} \tag{A15}$$

collecting terms, we can write $\gamma_k^< = \sum_{n=0}^N B_{k,n}^< \beta_n$, where

$$B_{k,n}^< = \frac{2k+1}{2} \sum_{m=0}^M \alpha_m \int_{-2}^0 dx\, P_k(x+1)$$
$$\times \int_{x-1}^{x+1} dt\, P_m(t) P_n(x-t)$$
$$= \frac{2k+1}{2} \sum_{m=0}^M \alpha_m \int_{-2}^0 dx\, P_k(x+1)(P_m * P_n)(x)$$
$$= \frac{2k+1}{2} \sum_{m=0}^M \alpha_m \int_{-1}^1 ds\, P_k(s)(P_m * P_n)(s-1). \quad (A16)$$

Using the Fourier expression for the Legendre convolution [Eq. (A10)], $B_{k,n}^<$ can be expressed in terms of spherical Bessel functions,

$$B_{k,n}^< = \frac{2k+1}{\pi} \sum_{m=0}^M (-i)^{m+n} \alpha_m \int_{-1}^1 ds\, P_k(s)$$
$$\times \int_{-\infty}^\infty d\omega\, e^{i\omega(s-1)} j_m(\omega) j_n(\omega). \quad (A17)$$

Consider the $B_{k,n+1}^<$ term, changing the order of integration and Fourier transforming the remaining Legendre polynomial give

$$B_{k,n+1}^< = \frac{2(2k+1)}{\pi} \sum_{m=0}^M (-i)^{m+n+1} i^k \alpha_m$$
$$\times \int_{-\infty}^\infty d\omega\, j_k(\omega) j_m(\omega) j_{n+1}(\omega) e^{-i\omega}. \quad (A18)$$

Applying the recursion relation of the spherical Bessel functions [Eq. (A11)] on n and k, we have

$$(-i)^{m+n+1} i^k j_k(\omega) j_m(\omega) j_{n+1}(\omega)$$
$$= (-i)^{m+n+1} i^k j_k(\omega) j_m(\omega) \left(\frac{2n+1}{\omega} j_n(\omega) - j_{n-1}(\omega) \right)$$
$$= \frac{2n+1}{2k+1} (-i)^{m+n+1} i^k \left(j_{k+1}(\omega) + j_{k-1}(\omega) \right) j_m(\omega) j_n(\omega)$$
$$+ (-i)^{m+n-1} i^k j_k(\omega) j_m(\omega) j_{n-1}(\omega). \quad (A19)$$

Back insertion in Eq. (A18) and simplifying prefactors in k give

$$B_{k,n+1}^< = -\frac{2n+1}{2k+3} B_{k+1,n}^< + \frac{2n+1}{2k-1} B_{k-1,n}^< + B_{k,n-1}^<. \quad (A20)$$

b. Second interval $x \in [0, 2]$

For $x \in [0, 2]$, we have $h(x) = h^>(x)$, where

$$h^>(x) = \int_{x-1}^1 dt\, f_M(t) g_N(x-t) = \sum_{k=0}^{M+N+1} \gamma_k^> P_k(x-1). \quad (A21)$$

$\gamma_k^>$ can be computed in the same way as $\gamma_k^<$ [see Eq. (A15)],

$$\gamma_k^> = \frac{2k+1}{2} \int_0^2 dx\, P_k(x-1) \int_{x-1}^1 dt\, f_M(t) g_N(x-t)$$
$$= \sum_{n=0}^N \beta_n \frac{2k+1}{2} \sum_{m=0}^M \alpha_m \int_0^2 dx\, P_k(x-1)$$
$$\times \int_{x-1}^1 dt\, P_m(t) P_n(x-t), \quad (A22)$$

collecting terms, we can write $\gamma_k^> = \sum_{n=0}^N B_{k,n}^> \beta_n$, where

$$B_{k,n}^> = \frac{2k+1}{2} \sum_{m=0}^M \alpha_m \int_0^2 dx\, P_k(x-1)$$
$$\times \int_{x-1}^1 dt\, P_m(t) P_n(x-t)$$
$$= \frac{2k+1}{2} \sum_{m=0}^M \alpha_m \int_0^2 dx\, P_k(x-1)(P_m * P_n)(x)$$
$$= \frac{2k+1}{2} \sum_{m=0}^M \alpha_m \int_{-1}^1 ds\, P_k(s)(P_m * P_n)(s+1). \quad (A23)$$

Using the Fourier expression for the Legendre convolution [Eq. (A10)] gives

$$B_{k,n}^> = \frac{2k+1}{\pi} \sum_{m=0}^M (-i)^{m+n} \alpha_m \int_{-1}^1 ds\, P_k(s)$$
$$\times \int_{-\infty}^\infty d\omega\, e^{i\omega(s+1)} j_m(\omega) j_n(\omega). \quad (A24)$$

Since the exponent in the integral is unchanged when applying the recursion relations of the spherical Bessel functions, we conclude that $B^>$ obeys the same recursion relation as $B^<$, albeit with a different starting point since the "seeding" integrals have a different sign in the exponent.

c. Summary

The convolution matrices for both intervals can be expressed as the integral sums,

$$B_{k,n}^{\lessgtr} = \frac{2(2k+1)}{\pi} \sum_{m=0}^M (-i)^{m+n} i^k \alpha_m$$
$$\times \int_{-\infty}^\infty d\omega\, j_k(\omega) j_m(\omega) j_n(\omega) e^{\mp i\omega}, \quad (A25)$$

differing only in the sign in the exponent. The coefficients are related by the recursion relation,

$$B_{k,n+1}^{\lessgtr} = -\frac{2n+1}{2k+3} B_{k+1,n}^{\lessgtr} + \frac{2n+1}{2k-1} B_{k-1,n}^{\lessgtr} + B_{k,n-1}^{\lessgtr}. \quad (A26)$$

In practice this recursion relation is only stable below the diagonal with $k > n$. To get entries above diagonal, the transpose relation that can be derived from the integral expression [Eq. (A18)], is used,

$$B_{k,n}^{\lessgtr} = (-1)^{n+k} \frac{2k+1}{2n+1} B_{n,k}^{\lessgtr}. \quad (A27)$$

3. Initial values $B_{k,0}^{\lessgtr}$ and $B_{k,1}^{\lessgtr}$

To start the recursion, the initial values for $n = 0$ and 1 are needed. To derive explicit expressions for these terms, we repeatedly use the Volterra integral formula for Legendre polynomials from Ref. 87,

$$S_{a,n}(x) = \int_a^x dt\, P_n(t), \quad (A28)$$
$$S_{a,0}(x) = x - a, \quad (A29)$$
$$S_{a,n}(x) = \frac{1}{2n+1} \left[P_{n+1}(t) - P_{n-1}(t) \right]_a^x, \quad (A30)$$

for $a = \pm 1$, we get

$$S_{\pm 1,0}(x) = x \mp 1 = P_1(x) \mp P_0(x), \tag{A31}$$

$$S_{\pm 1,n}(x) = \frac{1}{2n+1}[P_{n+1}(x) - P_{n-1}(x)], \tag{A32}$$

where we have used $P_n(\pm 1) = (\pm 1)^n$ to cancel the constant terms.

Returning to the convolution matrices, we have for $B_{k,n}^<$ and $n = 0$, using $P_0(x) = 1$,

$$
\begin{aligned}
B_{k,0}^{\lessgtr} &= \pm \frac{2k+1}{2} \sum_{m=0}^{M} \alpha_m \int_{-1}^{1} dx\, P_k(x) \int_{\mp 1}^{x} dt\, P_m(t) \\
&= \pm \frac{2k+1}{2} \sum_{m=0}^{M} \alpha_m \int_{-1}^{1} dx\, P_k(x) S_{\mp 1,m}(x) \\
&= \pm \frac{2k+1}{2} \sum_{m=0}^{M} \frac{\alpha_m}{2m+1} \int_{-1}^{1} dx\, P_k(x)[P_{m+1}(x) - P_{m-1}(x)],
\end{aligned}
\tag{A33}
$$

repeatedly using the Legendre orthogonality relation [Eq. (A6)] gives

$$
B_{k,0}^{\lessgtr} =
\begin{cases}
\alpha_0 \mp \frac{\alpha_1}{3}, & k = 0, \\
\pm\left(\frac{\alpha_{k-1}}{2k-1} - \frac{\alpha_{k+1}}{2k+3}\right), & k \geq 1.
\end{cases}
\tag{A34}
$$

For the second column with $n = 1$, we detail the derivation of $B_{k,1}^<$, the other case $B_{k,1}^>$ can be done analogously. Using $P_1(x) = x$, we get

$$
\begin{aligned}
B_{k,1}^< &= \frac{2k+1}{2} \sum_{m=0}^{M} \alpha_m \int_{-2}^{0} dx\, P_k(x+1) \int_{-1}^{x+1} dt\, P_m(t) P_1(x-t) \\
&= \frac{2k+1}{2} \sum_{m=0}^{M} \alpha_m \int_{-1}^{1} dx\, P_k(x) \int_{-1}^{x} dt\, P_m(t)(x-t-1) \\
&= -B_{k,0}^< + \frac{2k+1}{2} \sum_{m=0}^{M} \alpha_m \int_{-1}^{1} dx\, P_k(x) \int_{-1}^{x} dt\, P_m(t) \int_{t}^{x} ds \\
&= -B_{k,0}^< + \frac{2k+1}{2} \sum_{m=0}^{M} \alpha_m \int_{-1}^{1} dx\, P_k(x) r \int_{-1}^{x} ds \int_{-1}^{s} dt\, P_m(t),
\end{aligned}
\tag{A35}
$$

where the last step is obtained by changing the order of integration. The last integral relation is a double Volterra integral and can, hence, be written using $S_{-1,m}(x)$ as

$$
\begin{aligned}
B_{k,1}^< &= -B_{k,0}^< + \frac{2k+1}{2} \sum_{m=0}^{M} \alpha_m \int_{-1}^{1} dx\, P_k(x) \int_{-1}^{x} ds\, S_{-1,m}(s) \\
&= -B_{k,0}^< + \frac{1}{2} \sum_{m=0}^{M} \alpha_m \int_{-1}^{1} dx\,[P_{k-1}(x) - P_{k+1}(x)] S_{-1,m}(x), \quad \text{(A36)}
\end{aligned}
$$

where we, in the second step, have used partial integration and the Legendre derivative relation [Eq. (A7)].

For the second case $B_{k,1}^>$, the only difference is when we change the integration variable, we get $(x - t + 1)$, instead, of $(x - t - 1)$

in Eq. (A35), so the sign before $B_{k,0}$ is changed to $+1$. By using Eq. (A33), we obtain the recursion relation,

$$B_{k,1}^{\lessgtr} = \mp B_{k,0}^{\lessgtr} + \frac{B_{k-1,0}^{\lessgtr}}{2k-1} - \frac{B_{k+1,0}^{\lessgtr}}{2k+3}, \quad k \geq 1, \tag{A37}$$

with the special case for $k = 0$, $B_{0,1}^{\lessgtr} = \mp B_{1,0}^{\lessgtr}/3$.

REFERENCES

[1] A. A. Abrikosov, I. Dzyaloshinskii, L. P. Gorkov, and R. A. Silverman, *Methods of Quantum Field Theory in Statistical Physics* (Dover, New York, NY, 1975).

[2] R. Blankenbecler, D. J. Scalapino, and R. L. Sugar, "Monte Carlo calculations of coupled boson-fermion systems. I," Phys. Rev. D **24**, 2278–2286 (1981).

[3] A. Georges, G. Kotliar, W. Krauth, and M. J. Rozenberg, "Dynamical mean-field theory of strongly correlated fermion systems and the limit of infinite dimensions," Rev. Mod. Phys. **68**, 13–125 (1996).

[4] A. Toschi, A. A. Katanin, and K. Held, "Dynamical vertex approximation: A step beyond dynamical mean-field theory," Phys. Rev. B **75**, 045118 (2007).

[5] A. N. Rubtsov, M. I. Katsnelson, and A. I. Lichtenstein, "Dual fermion approach to nonlocal correlations in the Hubbard model," Phys. Rev. B **77**, 033101 (2008).

[6] T. Maier, M. Jarrell, T. Pruschke, and M. H. Hettler, "Quantum cluster theories," Rev. Mod. Phys. **77**, 1027–1080 (2005).

[7] N. Prokof'ev and B. Svistunov, "Bold diagrammatic Monte Carlo technique: When the sign problem is welcome," Phys. Rev. Lett. **99**, 250201 (2007).

[8] M. Kaltak, J. Klimeš, and G. Kresse, "Low scaling algorithms for the random phase approximation: Imaginary time and Laplace transformations," J. Chem. Theory Comput. **10**, 2498–2507 (2014).

[9] P. García-González and R. W. Godby, "Self-consistent calculation of total energies of the electron gas using many-body perturbation theory," Phys. Rev. B **63**, 075112 (2001).

[10] N. E. Dahlen and R. van Leeuwen, "Self-consistent solution of the Dyson equation for atoms and molecules within a conserving approximation," J. Chem. Phys. **122**, 164102 (2005).

[11] J. J. Phillips and D. Zgid, "Communication: The description of strong correlation within self-consistent Green's function second-order perturbation theory," J. Chem. Phys. **140**, 241101 (2014).

[12] J. J. Phillips, A. A. Kananenka, and D. Zgid, "Fractional charge and spin errors in self-consistent Green's function theory," J. Chem. Phys. **142**, 194108 (2015).

[13] A. A. Kananenka, J. J. Phillips, and D. Zgid, "Efficient temperature-dependent Green's functions methods for realistic systems: Compact grids for orthogonal polynomial transforms," J. Chem. Theory Comput. **12**, 564–571 (2016).

[14] A. A. Kananenka, A. R. Welden, T. N. Lan, E. Gull, and D. Zgid, "Efficient temperature-dependent Green's function methods for realistic systems: Using cubic spline interpolation to approximate Matsubara Green's functions," J. Chem. Theory Comput. **12**, 2250–2259 (2016).

[15] A. A. Rusakov and D. Zgid, "Self-consistent second-order Green's function perturbation theory for periodic systems," J. Chem. Phys. **144**, 054106 (2016).

[16] A. R. Welden, A. A. Rusakov, and D. Zgid, "Exploring connections between statistical mechanics and Green's functions for realistic systems: Temperature dependent electronic entropy and internal energy from a self-consistent second-order Green's function," J. Chem. Phys. **145**, 204106 (2016).

[17] S. Iskakov, A. A. Rusakov, D. Zgid, and E. Gull, "Effect of propagator renormalization on the band gap of insulating solids," Phys. Rev. B **100**, 085112 (2019).

[18] L. Hedin, "New method for calculating the one-particle Green's function with application to the electron-gas problem," Phys. Rev. **139**, A796–A823 (1965).

[19] F. Aryasetiawan and O. Gunnarsson, "The *GW* method," Rep. Prog. Phys. **61**, 237–312 (1998).

[20] A. Stan, N. E. Dahlen, and R. van Leeuwen, "Levels of self-consistency in the *GW* approximation," J. Chem. Phys. **130**, 114105 (2009).

[21] A. Kutepov, S. Y. Savrasov, and G. Kotliar, "Ground-state properties of simple elements from GW calculations," Phys. Rev. B **80**, 041103 (2009).

[22] M. J. van Setten, F. Caruso, S. Sharifzadeh, X. Ren, M. Scheffler, F. Liu, J. Lischner, L. Lin, J. R. Deslippe, S. G. Louie, C. Yang, F. Weigend, J. B. Neaton,

F. Evers, and P. Rinke, "$GW100$: Benchmarking G_0W_0 for molecular systems," J. Chem. Theory Comput. **11**, 5665–5687 (2015).

[23]E. Maggio, P. Liu, M. J. van Setten, and G. Kresse, "$GW100$: A plane wave perspective for small molecules," J. Chem. Theory Comput. **13**, 635–648 (2017).

[24]M. Grumet, P. Liu, M. Kaltak, J. Klimeš, and G. Kresse, "Beyond the quasiparticle approximation: Fully self-consistent GW calculations," Phys. Rev. B **98**, 155143 (2018).

[25]A. L. Kutepov, "Electronic structure of Na, K, Si, and LiF from self-consistent solution of Hedin's equations including vertex corrections," Phys. Rev. B **94**, 155101 (2016).

[26]A. L. Kutepov, "Self-consistent solution of Hedin's equations: Semiconductors and insulators," Phys. Rev. B **95**, 195120 (2017).

[27]A. A. Kananenka, E. Gull, and D. Zgid, "Systematically improvable multiscale solver for correlated electron systems," Phys. Rev. B **91**, 121111 (2015).

[28]T. N. Lan, A. A. Kananenka, and D. Zgid, "Communication: Towards ab initio self-energy embedding theory in quantum chemistry," J. Chem. Phys. **143**, 241102 (2015).

[29]D. Zgid and E. Gull, "Finite temperature quantum embedding theories for correlated systems," New J. Phys. **19**, 023047 (2017).

[30]T. N. Lan and D. Zgid, "Generalized self-energy embedding theory," J. Phys. Chem. Lett. **8**, 2200–2205 (2017).

[31]T. N. Lan, A. Shee, J. Li, E. Gull, and D. Zgid, "Testing self-energy embedding theory in combination with GW," Phys. Rev. B **96**, 155106 (2017).

[32]L. N. Tran, S. Iskakov, and D. Zgid, "Spin-unrestricted self-energy embedding theory," J. Phys. Chem. Lett. **9**, 4444–4450 (2018).

[33]A. A. Rusakov, S. Iskakov, L. N. Tran, and D. Zgid, "Self-energy embedding theory (SEET) for periodic systems," J. Chem. Theory Comput. **15**, 229–240 (2019).

[34]D. E. Taylor, J. G. Ángyán, G. Galli, C. Zhang, F. Gygi, K. Hirao, J. W. Song, K. Rahul, O. Anatole von Lilienfeld, R. Podeszwa, I. W. Bulik, T. M. Henderson, G. E. Scuseria, J. Toulouse, R. Peverati, D. G. Truhlar, and K. Szalewicz, "Blind test of density-functional-based methods on intermolecular interaction energies," J. Chem. Phys. **145**, 124105 (2016).

[35]G. Chalasinski and M. M. Szczesniak, "Origins of structure and energetics of van der Waals clusters from ab initio calculations," Chem. Rev. **94**, 1723–1765 (1994).

[36]G. Chalasinski and M. M. Szczesniak, "State of the art and challenges of the ab initio theory of intermolecular interactions," Chem. Rev. **100**, 4227–4252 (2000).

[37]G. Chalasinski and M. Gutowski, "Weak interactions between small systems. models for studying the nature of intermolecular forces and challenging problems for ab initio calculations," Chem. Rev. **88**, 943–962 (1988).

[38]R. Podeszwa, R. Bukowski, and K. Szalewicz, "Potential energy surface for the benzene dimer and perturbational analysis of π–π interactions," J. Phys. Chem. A **110**, 10345–10354 (2006).

[39]S. Sharma, K. Sivalingam, F. Neese, and G. K.-L. Chan, "Low-energy spectrum of iron-sulfur clusters directly from many-particle quantum mechanics," Nat. Chem. **6**, 927–933 (2014).

[40]Z. Li, S. Guo, Q. Sun, and G. K.-L. Chan, "Electronic landscape of the P-cluster of nitrogenase as revealed through many-electron quantum wavefunction simulations," Nat. Chem. **11**, 1026–1033 (2019).

[41]T. Matsubara, "A new approach to quantum-statistical mechanics," Prog. Theor. Phys. **14**, 351–378 (1955).

[42]N. Blümer, "Mott-Hubbard metal-insulator transition and optical conductivity in high dimensions," Ph.D. thesis, Universität Augsburg, 2002.

[43]A.-B. Comanac, "Dynamical mean field theory of correlated electron systems: New algorithms and applications to local observables," Ph.D. thesis, Columbia University, 2007.

[44]D. Hügel, P. Werner, L. Pollet, and H. U. R. Strand, "Bosonic self-energy functional theory," Phys. Rev. B **94**, 195119 (2016).

[45]W. Ku and A. G. Eguiluz, "Band-gap problem in semiconductors revisited: Effects of core states and many-body self-consistency," Phys. Rev. Lett. **89**, 126401 (2002).

[46]W. Ku, "Electronic excitations in metals and semiconductors: Ab initio studies of realistic many-particle systems," Ph.D. thesis, University of Tennessee, 2000.

[47]L. Boehnke, H. Hafermann, M. Ferrero, F. Lechermann, and O. Parcollet, "Orthogonal polynomial representation of imaginary-time Green's functions," Phys. Rev. B **84**, 075145 (2011).

[48]E. Gull, S. Iskakov, I. Krivenko, A. A. Rusakov, and D. Zgid, "Chebyshev polynomial representation of imaginary-time response functions," Phys. Rev. B **98**, 075127 (2018).

[49]H. Shinaoka, J. Otsuki, M. Ohzeki, and K. Yoshimi, "Compressing Green's function using intermediate representation between imaginary-time and real-frequency domains," Phys. Rev. B **96**, 035147 (2017).

[50]N. Chikano, J. Otsuki, and H. Shinaoka, "Performance analysis of a physically constructed orthogonal representation of imaginary-time Green's function," Phys. Rev. B **98**, 035104 (2018).

[51]N. Chikano, K. Yoshimi, J. Otsuki, and H. Shinaoka, "irbasis: Open-source database and software for intermediate-representation basis functions of imaginary-time Green's function," Comput. Phys. Commun. **240**, 181–188 (2019).

[52]J. Li, M. Wallerberger, N. Chikano, C.-N. Yeh, E. Gull, and H. Shinaoka, "Sparse sampling approach to efficient ab initio calculations at finite temperature," Phys. Rev. B **101**, 035144 (2020).

[53]M. Kaltak and G. Kresse, "Minimax isometry method," arXiv:1909.01740 [cond-mat.mtrl-sci] (2019).

[54]J. W. Negele and H. Orland, *Quantum Many-Particle Systems* (Westview Press, 1998).

[55]A. L. Fetter and J. D. Walecka, *Quantum Theory of Many-Particle Systems* (Dover Publications, Inc., Mineloa, NY, 2003).

[56]A. Altland and B. Simons, *Condensed Matter Field Theory*, 2nd ed. (Cambridge University Press, Cambridge, UK, 2010).

[57]G. Stefanucci and R. van Leeuwen, *Nonequilibrium Many-Body Theory of Quantum Systems: A Modern Introduction* (Cambridge University Press, 2013).

[58]M. Schüler and Y. Pavlyukh, "Spectral properties from Matsubara Green's function approach: Application to molecules," Phys. Rev. B **97**, 115164 (2018).

[59]P. D. Lax, *Functional Analysis* (John Wiley & Sons, Inc., 2002).

[60]O. Parcollet, M. Ferrero, T. Ayral, H. Hafermann, I. Krivenko, L. Messio, and P. Seth, "TRIQS: A toolbox for research on interacting quantum systems," Comput. Phys. Commun. **196**, 398–415 (2015).

[61]L.-L. W. Jie Shen and T. Tang, *Spectral Methods Algorithms, Analysis and Applications*, Springer Series in Computational Mathematics Vol. 41 (Springer, 2011).

[62]N. Hale and A. Townsend, "An algorithm for the convolution of Legendre series," SIAM J. Sci. Comput. **36**, A1207–A1220 (2014).

[63]T. T. Jie Shen, in *Spectral and High-Order Methods With Applications*, Mathematics Monograph Series 3, edited by C. Yuzhuo (Science Press, Beijing, 2006).

[64]D. Neuhauser, R. Baer, and D. Zgid, "Stochastic self-consistent second-order Green's function method for correlation energies of large electronic systems," J. Chem. Theory Comput. **13**, 5396–5403 (2017).

[65]Q. Sun, T. C. Berkelbach, N. S. Blunt, G. H. Booth, S. Guo, Z. Li, J. Liu, J. D. McClain, E. R. Sayfutyarova, S. Sharma, S. Wouters, and G. K. L. Chan, "PySCF: The python-based simulations of chemistry framework," Wiley Interdiscip. Rev.: Comput. Mol. Sci. **8**, e1340 (2018).

[66]This follows from the generalized imaginary time trace $\text{Tr}[G] \equiv \frac{-\xi}{\beta} \sum_{ab} \iint_0^\beta d\tau d\tau' \, \delta_{a,b} \delta(\tau - \tau' + 0^-) G_{ab}(\tau, \tau')$ of a response function $G_{ab}(\tau, \tau') \equiv -\langle \mathcal{T} c_a(\tau) c_b^\dagger(\tau') \rangle$.

[67]S. Boys and F. Bernardi, "The calculation of small molecular interactions by the differences of separate total energies. Some procedures with reduced errors," Mol. Phys. **19**, 553–566 (1970).

[68]T. Van Mourik, A. K. Wilson, and T. H. Dunning, "Benchmark calculations with correlated molecular wavefunctions. XIII. Potential energy curves for He$_2$, Ne$_2$ and Ar$_2$ using correlation consistent basis sets through augmented sextuple zeta," Mol. Phys. **96**, 529–547 (1999).

[69] L. J. Holleboom and J. G. Snijders, "A comparison between the Møller–Plesset and Green's function perturbative approaches to the calculation of the correlation energy in the many-electron problem," J. Chem. Phys. **93**, 5826–5837 (1990).

[70] D. Feller, "Application of systematic sequences of wave functions to the water dimer," J. Chem. Phys. **96**, 6104–6114 (1992).

[71] T. Helgaker, W. Klopper, H. Koch, and J. Noga, "Basis-set convergence of correlated calculations on water," J. Chem. Phys. **106**, 9639–9646 (1997).

[72] R. A. Kendall, T. H. Dunning, and R. J. Harrison, "Electron affinities of the first-row atoms revisited. Systematic basis sets and wave functions," J. Chem. Phys. **96**, 6796–6806 (1992).

[73] D. E. Woon and T. H. Dunning, "Gaussian basis sets for use in correlated molecular calculations. III. The atoms aluminum through argon," J. Chem. Phys. **98**, 1358–1371 (1993).

[74] D. E. Woon and T. H. Dunning, "Gaussian basis sets for use in correlated molecular calculations. IV. Calculation of static electrical response properties," J. Chem. Phys. **100**, 2975–2988 (1994).

[75] D. E. Woon and T. H. Dunning, "Benchmark calculations with correlated molecular wave functions. I. Multireference configuration interaction calculations for the second row diatomic hydrides," J. Chem. Phys. **99**, 1914–1929 (1993).

[76] D. E. Woon and T. H. Dunning, "Calculation of the electron affinities of the second row atoms: Al–Cl," J. Chem. Phys. **99**, 3730–3737 (1993).

[77] D. E. Woon, "Accurate modeling of intermolecular forces: A systematic Møller-Plesset study of the argon dimer using correlation consistent basis sets," Chem. Phys. Lett. **204**, 29–35 (1993).

[78] K. A. Peterson, R. A. Kendall, and T. H. Dunning, "Benchmark calculations with correlated molecular wave functions. II. Configuration interaction calculations on first row diatomic hydrides," J. Chem. Phys. **99**, 1930–1944 (1993).

[79] S. S. Xantheas and T. H. Dunning, "Theoretical studies of sulfurous species of importance in atmospheric chemistry. 1. Characterization of the mercaptooxy (HSO) and hydroxythio (SOH) isomers," J. Phys. Chem. **97**, 6616–6627 (1993).

[80] D. E. Woon, "Benchmark calculations with correlated molecular wave functions. V. The determination of accurate ab initio intermolecular potentials for He_2, Ne_2, and Ar_2," J. Chem. Phys. **100**, 2838–2850 (1994).

[81] D. E. Woon and T. H. Dunning, "Benchmark calculations with correlated molecular wave functions. VI. Second row A_2 and first row/second row AB diatomic molecules," J. Chem. Phys. **101**, 8877–8893 (1994).

[82] D. E. Woon, T. H. Dunning, and K. A. Peterson, "Ab initio investigation of the N_2–HF complex: Accurate structure and energetics," J. Chem. Phys. **104**, 5883–5891 (1996).

[83] T. van Mourik and T. H. Dunning, "Ab initio characterization of the structure and energetics of the ArHF complex," J. Chem. Phys. **107**, 2451–2462 (1997).

[84] K. A. Peterson and T. H. Dunning, "The CO molecule: The role of basis set and correlation treatment in the calculation of molecular properties," J. Mol. Struct.: THEOCHEM **400**, 93–117 (1997), ab initio benchmark studies.

[85] K. A. Peterson, A. K. Wilson, D. E. Woon, and T. H. Dunning, Jr., "Benchmark calculations with correlated molecular wave functions XII. Core correlation effects on the homonuclear diatomic molecules B_2-F_2," Theor. Chem. Acc. **97**, 251–259 (1997).

[86] Y. Katznelson, Fundamental Principles of Optical Lithography (Dover, 1976).

[87] A. R. DiDonato, "Recurrence relations for the indefinite integrals of the associated Legendre functions," Math. Comput. **38**, 547–551 (1982).

05 July 2024 10:32:15